DDX3X/MAVS alleviates doxorubicin-induced cardiotoxicity by regulating stress granules

KAIXIANG ZHAO[1], SHAOCHEN WANG[1], DANDAN FENG[2],
DONGWEI WANG[1], GUANG YANG[1] and FANGFANG LANG[3]

[1]Department of Cardiology, The First Affiliated Hospital of Shandong First Medical University (Shandong Provincial Qianfoshan Hospital), Jinan, Shandong 250014, P.R China; [2]Department of Cardiology, Shandong First Medical University, Jinan, Shandong 250017, P.R. China; [3]Department of Obstetrics and Gynecology, Maternal and Child Health Hospital of Shandong Province, Jinan, Shandong 250013, P.R. China

Abstract. The specific mechanisms of doxorubicin (Dox)-induced cardiotoxicity (DIC) remain unclear. In the present study, H9c2 cardiomyocytes were treated with Dox, and it was revealed that DEAD-box RNA helicase 3 X-linked (DDX3X), mitochondrial antiviral signaling (MAVS) and stress granules (SGs) were present at lower levels in the treated H9c2 cardiomyocytes compared with those in the control cells. The present study further investigated the mechanisms through which DIC occurs. Pretreatment with arsenite, which pharmacologically accelerates SGs, alleviated the myocardial injury caused by Dox. By contrast, anisomycin, an SG inhibitor, increased cardiomyocyte apoptosis induced by Dox. In addition, both DDX3X knockdown and pretreatment with RK-33 (a DDX3X pharmacological inhibitor) decreased SG expression, whereas DDX3X overexpression promoted SG generation. These results indicated that DDX3X mitigated DIC through the regulation of SGs. In addition, MAVS knockdown inhibited SG assembly and reduced the expression of the anti-apoptotic inhibitor Bcl2, and MAVS was influenced by DDX3X, thereby serving as a connector between DDX3X and SGs. The results from western blotting, reverse transcription-quantitative PCR, immunofluorescence and flow cytometry analysis demonstrated that DDX3X, MAVS, and SGs may serve as key protective factors in DIC.

Correspondence to: Professor Guang Yang, Department of Cardiology, The First Affiliated Hospital of Shandong First Medical University (Shandong Provincial Qianfoshan Hospital), 16766 Jingshi Road, Jinan, Shandong 250014, P.R. China
E-mail: yangg1972@126.com

Professor Fangfang Lang, Department of Obstetrics and Gynecology, Maternal and Child Health Hospital of Shandong Province, 238 Jingshi East Road, Jinan, Shandong 250013, P.R. China
E-mail: langff77@163.com

Introduction

Anthracycline drugs such as doxorubicin (Dox) interfere with DNA synthesis by embedding itself into the double-stranded DNA and inhibiting topoisomerase II, thus exerting antitumor effects (1-4). Dox is important in clinical practice due to its precision and efficacy in treating solid tumors and hematological malignancies. However, Dox has multiple side effects, such as myelosuppression, neurological disturbances, hair loss and cardiotoxicity, which is the most serious effect (5-8). Dox-induced cardiotoxicity (DIC) is dose-dependent, and the incidence of congestive heart failure is proportional to the dose of Dox (9). Left ventricular ejection fraction continues to decline as a characteristic of DIC; however, patients may have no symptoms in the early stages. Clinical manifestations can occur years later and are difficult to treat (10,11). Dox has a high affinity for cardiolipin in the inner mitochondrial membrane, and the mitochondrial density of the heart is higher than that of the majority of other tissues, making the heart the main target of Dox (12-14). Dox is a potent oxidant that produces reactive oxygen species (ROS) through the NADH dehydrogenase in the mitochondria, damaging normal mitochondrial function (15,16). Glutathione peroxidase 1 (GPx1) antagonizes ROS, and the P/O ratio of mitochondria in GPx1-deficient mice is decreased compared with that of controls; the hearts of such mice are more susceptible to Dox-induced damage (17-19). The specific mechanism of DIC remains unclear although various theories, such as those involving oxidative stress, calcium overload and iron metabolism disorder, have been proposed. The present study considered DEAD-box RNA helicase 3 X-linked (DDX3X), mitochondrial antiviral signaling (MAVS) and stress granules (SGs) to further explore the molecular mechanisms of DIC.

DDX3X is a member of the DEAD-box helicase family in superfamily 2. The two RecA-like domains in the helicase core contain 12 characteristic conserved motifs, which form RNA substrate channels that bind to ligands such as ATP (20,21). DDX3X has become a research hotspot for a variety of diseases, such as nervous system diseases, viral infection and inflammatory disorders, because DDX3X is involved in a variety of RNA metabolic processes, such as pre-mRNA splicing, ribosome biogenesis, mRNA translation initiation

and RNA decay (22-27). DDX3X enables nucleocytoplasmic shuttling via interacting with chromosomal maintenance 1 and nuclear RNA export factor 1, which are associated with the development of tumors (28,29). In addition, DDX3X promotes the spread of cancer cells by enhancing RAC1 signaling and SG assembly, and upregulating other pathways (30,31). The phosphorylation and ubiquitination of DDX3X serve important roles in the antiviral process, such as DDX3X phosphorylation under the action of IKKε or TANK-binding kinase 1. NLR family pyrin domain containing (NLRP)11 can weaken the IKKε-mediated phosphorylation of DDX3X, resulting in reductions in type I interferon induction after viral infection (32-34). DDX3X induces pyroptosis by promoting NLRP3 activation, whereas the assembly of SGs leads to DDX3X isolation, thereby inhibiting NLRP3 activation (35).

MAVS has a key role in host resistance to viral infections. MAVS is localized to the mitochondrial outer membrane via the C-terminal transmembrane domain and is directly associated with the C-terminus of DDX3X via the N-terminal caspase recruitment domain. MAVS thus enhances the activation of RIG-I-like receptor (RLR) antiviral signaling (36). MAVS carries out an antiviral role by activating protein kinase R (PKR), which recruits PKR to dsRNA-induced SGs (37). The RNA-binding protein nudix hydrolase 21 physically associates with MAVS and mediates its localization to SGs, inducing interferon production (38). Research on the role of MAVS in cardiovascular disease is scarce. MAVS-deficient mice have decreased cardiac function and ventricular dilation, and the nucleotide binding oligomerization domain 1/receptor-interacting protein 2/MAVS trigonal signaling complex carries out an important role in hypertrophic myocardial remodeling (39).

SGs are reversible membraneless cytoplasmic compartments that enable cells to resist damage from various stressors, such as oxidative or endoplasmic reticulum stress, heat shock, viral infections, toxic drugs, arsenite (Ar) and X-rays (40-42). SGs protect mRNA and proteins from external stress through liquid-liquid phase separation (LLPS) (43,44). Key proteins such as ras GTPase-activating protein-binding protein 1 (G3BP1), cytotoxic granule-associated RNA binding protein 1 and polyadenylate-binding protein 1 bind to mRNA in the nucleus to form messenger ribonucleoprotein, which is transferred to the cytoplasm as the core of SGs. The SG kernel is further fused through protein-protein interactions and forms a liquid shell through the microtubule structure. The SG shell and core are relatively dynamic and stable, respectively (45-47). Imbalances in the assembly and disassembly of SGs are associated with a variety of diseases, such as neurodegenerative diseases, viral infections and cancer (48-51).

Notably, SGs have a cardioprotective effect. CUG binding protein 2 contributes to homeostasis in H9c2 cells by promoting the coordinated translocation of cyclooxygenase-2 mRNA to SGs (52). G3BP1 controls the genes required for cardiomyocyte growth by negatively regulating microRNA-1 (53). In a model of arrhythmia, G3BP1 overexpression has been shown to substantially reduce ROS levels and calcium overload in HL-1 cells with atrial fibrillation (54). In addition, SGs are resistant to viral myocarditis and septic cardiomyopathy (55,56). However, to the best of our knowledge, neither SGs nor MAVS have been investigated in DIC.

MAVS and SGs have cardioprotective effects, and DDX3X is their positive regulator; therefore, the present study assessed the relationship and influence of DDX3X, MAVS and SGs on DIC. H9c2 cells were induced with Dox for 24 h to construct a DIC model. In the DIC model, the present study examined alterations in the anti-apoptotic marker Bcl-2 through inhibition of DDX3X, suppression of SGs, and knockdown of MAVS. These findings provide insights into the molecular mechanisms of DIC and suggest a therapeutic target for DIC.

Materials and methods

Cell culture, reagents and transfection. H9c2 cells (cat. no. CL-0089; Wuhan Pricella Biotechnology, Ltd; https://m.procell.com.cn/view/690.html) were cultured in a humidified atmosphere at 37°C and 5% CO_2 using complete medium consisting of DMEM (cat. no. C3113-0500; Shanghai VivaCell Biosciences, Ltd.), 10% fetal bovine serum (cat. no. FSP500; Shanghai ExCell Biology, Inc.) and 1% penicillin/streptomycin (cat. no. C3420-0100; Shanghai VivaCell Biosciences, Ltd.). Dox (cat. no. HY-15142; MedChemExpress) was administered to H9c2 cells at a concentration of 2 μmol/l and incubated at 37°C for 24 h. The negative control (NC) group received no drug treatment. RK-33 (cat. no. S8246; Selleck Chemicals) was administered at 5 μmol/l with the following protocol: H9c2 cells were pretreated with RK-33 for 30 min at 37°C, then co-treated with Dox for 24 h. The NC group received Dox treatment alone for 24 h. Anisomycin (An; cat. no. S17105; Shanghai Yuanye Biotechnology; https://www.shyuanye.com/goods-S17105.html) was used at 20 ng/ml with the following treatment protocol: H9c2 cells were pretreated with An for 30 min at 37°C followed by 24 h co-incubation with Dox. The NC group received Dox treatment alone for 24 h. Ar (cat. no. S463149; Shanghai Aladdin Biochemical Technology) was administered at 10 μmol/l under the following conditions: After 12 h of Dox treatment, H9c2 cells were co-treated with Ar and Dox for an additional 12 h at 37°C. The NC group received Dox treatment alone for 24 h.

H9c2 cells at 85% confluency were transfected for 24 h at 37°C with 2.5 μg DDX3X pcDNA3.1-3xFlag-C or negative control plasmids (Research Cloud, http://www.keyybio.com/) using Lipo8000 (cat. no. C0533; Beyotime Institute of Biotechnology), followed immediately by 24 h treatment with 2 μmol/l Dox at 37°C. In addition, H9c2 cells at 85% confluency were transfected with 50 nM DDX3X, MAVS, or nontargeting scramble small interfering (si) RNA (GENECREATE, https://www.genecreate.cn/) using Lipo8000 transfection reagent at 37°C for 24 h. Nontargeting scramble siRNA was used as negative control. Immediately following transfection, cells were treated with 2 μmol/l Dox for 24 h at 37°C. The siRNA sequences are shown in Table I.

Detection of protein expression by western blotting. H9c2 cells were lysed on ice using RIPA Lysis Buffer (cat. no. P0013B; Beyotime Institute of Biotechnology) for 10 min, after which, they were disrupted three times (12 sec/pulse; 20% power; 4°C) using an ultrasonic disruptor (cat. No JY88-IIN; Ningbo Scientz Biotechnology Co., Ltd.) and centrifuged at 12,000 x g for 5 min at 4°C to remove cell debris. Protein concentration was detected using a BCA Protein Assay

Table I. siRNA sequences.

Gene	Sequence (5'-3')
DDX3X siRNA	Sense, GGAGGAUUUCUUAUACCAUTT
	Antisense, AUGGUAUAAGAAAUCCUCCTT
MAVS siRNA	Sense, GGUCACAGUAUCAGCUCUA
	Antisense, UAGAGCUGAUACUGUGACC
Negative control siRNA	Sense, UUCUCCGAACGUGUCACGUTT
	Antisense, ACGUGACACGUUCGGAGAATT

DDX3X, DEAD-box RNA helicase 3 X-linked; MAVS, mitochondrial antiviral signaling; siRNA, small interfering RNA.

Kit (cat. no. P0012S; Beyotime Institute of Biotechnology). Protein loading buffer (cat. no. P0015; Beyotime Institute of Biotechnology) was then added, mixed and boiled for 10 min. Total protein (20-50 μg) was subsequently separated by SDS-PAGE on 12.5% gels (cat. no. PG113; Epizyme; Ipsen Pharma) and transferred to 0.45-μm PVDF membranes (cat. no. IPVH00010; MilliporeSigma). The PVDF membranes were blocked with 5% skim milk powder at room temperature for 2 h, incubated with specific primary antibodies at 4˚C overnight, washed three times with TBS containing 0.1% Tween-20 and incubated with HRP-conjugated secondary antibodies at room temperature for 1 h. The blots were visualized using ECL Enhanced Plus Kit (cat. no. RM00021P; ABclonal Biotech Co., Ltd.), images were acquired using a gel imager (ChemiDoc; Bio-Rad Laboratories, Inc.) and image grayscale values were analyzed using ImageJ v1.8.0.112 software (National Institutes of Health). The primary antibodies used were as follows: Anti-DDX3 antibody (1:1,000; cat. no. ab196032; Abcam), anti-G3BP1 polyclonal antibody (1:10,000; cat. no. 13057-2-AP; Proteintech Group, Inc.), anti-MAVS polyclonal antibody (1:10,000; cat. no. 14341-1-AP; Proteintech Group, Inc.), anti-Bcl2 polyclonal antibody (1:1,000; cat. no. 26593-1-AP; Proteintech Group, Inc.) and anti-GAPDH polyclonal antibody (1:10,000; cat. no. 10494-1-AP; Proteintech Group, Inc.). The following secondary antibodies were used: HRP-conjugated Goat Anti-Rabbit IgG (1:10,000; cat. no. SA00001-2; Proteintech Group, Inc.) and HRP-conjugated Goat Anti-Mouse IgG (1:10,000; cat. no. SA00001-1; Proteintech Group, Inc.).

Detection of mRNA expression by reverse transcription-quantitative PCR (RT-qPCR). Total RNA Isolation Kit V2 (cat. no. RC112-01; Vazyme Biotech Co., Ltd.) was used to extract total RNA from each group of cells. RNA concentration and purity were determined using a spectrophotometer (cat. no. SMA4000; Merinton Instrument, Ltd.). RNA was then reverse transcribed into cDNA using Hifair III 1st Strand cDNA Synthesis SuperMix for qPCR (cat. no. 11141ES60; Shanghai Yeasen Biotechnology Co., Ltd.) following the manufacturer's protocol. Hieff qPCR SYBR Green Master Mix (cat. no. 11201ES60; Shanghai Yeasen Biotechnology Co., Ltd.) was used to perform qPCR on the obtained cDNA. The thermocycling conditions were as follows: 95˚C for 30 sec; followed by 40 cycles at 95˚C 10 sec and 60˚C 30 sec. Fluorescent quantitative detection was carried out using the

CFX96 RT-qPCR instrument (Bio-Rad Laboratories, Inc.) and quantitative analysis was performed using the $2^{-\Delta\Delta Cq}$ method (57). Primer sequences used for RT-qPCR are listed in Table II.

Immunofluorescence detection of SGs. Cells were fixed with 4% paraformaldehyde (cat. no. BL539A; Biosharp Life Sciences) for 15 min at room temperature, washed three times with PBS (cat. no. P1020; Beijing Solarbio Science & Technology Co., Ltd.) and permeabilized with Triton X-100 (cat. no. P0096; Beyotime Institute of Biotechnology) for 20 min at room temperature. After washing three times with PBS, the cells were blocked with goat serum (cat. no. C0265; Beyotime Institute of Biotechnology) for 1 h at room temperature and were then incubated with a specific G3BP1 polyclonal antibody (1:1,000; cat. no. 13057-2-AP; Proteintech Group, Inc.) overnight at 4˚C. After washing three times with PBS, the cells were incubated with a CoraLite488-conjugated Goat Anti-Rabbit IgG secondary antibody (1:1,000; cat. no. SA00013-2; Proteintech Group Inc.) for 1 h at room temperature. After a further three washes with PBS, cell nuclei were stained with DAPI (1:1,000; cat. no. C1002; Beyotime Institute of Biotechnology) for 5 min at room temperature and the cells were imaged using a fluorescence microscope (Leica Microsystems GmbH).

Detection of apoptosis rate using flow cytometry. The Annexin V-FITC/PI apoptosis detection kit (cat. no. 40302ES60; Shanghai Yeasen Biotechnology Co., Ltd.) was used to detect levels of apoptosis. After 24 h treatment with 2 μmol/l Dox, H9c2 cells were digested with 0.25% EDTA-free Trypsin (cat. no. T1350; Beijing Solarbio Science & Technology Co., Ltd.) and then centrifuged at 300 x g and 4˚C for 5 min to collect ~200,000 cells. The cells were washed with precooled PBS twice and centrifuged at 300 x g and 4˚C for 5 min each time. After resuspension with 100 μl 1X binding buffer, the cells were treated with 5 μl Annexin V-FITC and 10 μl PI staining solution at room temperature for 15 min in the dark. After 400 μl binding buffer was added, the early and late apoptosis rate of cells was detected by a FACSAria™ II cell sorter (BD Biosciences). The data were analyzed using FlowJo_v10.8.1 software (FlowJo; BD Biosciences).

Cell viability assay. H9c2 cells were seeded into 96-well plates at 1,000 cells/well and incubated at 37˚C for 24 h. The

Table II. Primer sequences used for quantitative PCR.

Gene	Sequence (5'-3')
GAPDH	Forward, GTATTGGGCGCCTGGTCACC
	Reverse, CGCTCCTGGAAGATGGTGATGG
DDX3X	Forward, GAGAAAAGAGACTTGATGGCTTGTG
	Reverse, ATCTGACTCAAGATGGGCAAGAG
G3BP1	Forward, ATGAGGTCTTCGGTGGCTTTG
	Reverse, ATGTTCCTCCAAGTCATTGCTAAC
MAVS	Forward, GTCCCCAGTAGAGAATTCGGA
	Reverse, CCCAGTTCGGGTTCTTGCTC

DDX3X, DEAD-box RNA helicase 3 X-linked; G3BP1, ras GTPase-activating protein-binding protein 1; MAVS, mitochondrial antiviral signaling.

cells were stimulated with 10 μmol/l Ar at 37°C for various durations (0, 12, 24 and 48 h), and then cell viability was assessed using a Cell Counting Kit-8 (CCK-8; cat. no. K1018; APExBIO Technology LLC.) with 4 h incubation at 37°C. The optical density value was measured using an enzyme-labeling instrument at a wavelength of 450 nm.

Statistical analysis. Data analysis was performed using GraphPad Prism 9.0 software (Dotmatics). Statistical significance was determined using an unpaired Student's t-test (for 2 groups) or one-way ANOVA with Tukey's multiple comparisons test (≥3 groups). All data are presented as the mean ± SEM and all experiments were repeated at least three times. $P<0.05$ was considered to indicate a statistically significant difference.

Results

DDX3X and SGs are downregulated in Dox-induced H9c2 cells. H9c2 cells were treated with 2 μmol/l Dox for 24 h to induce myocardial injury (58-60). Flow cytometry analysis revealed that the apoptotic rate of H9c2 cardiomyocytes was increased after 24 h of Dox treatment (Fig. 1A). Western blotting revealed the anti-apoptotic marker Bcl2 was downregulated after treatment (Fig. 1B). Next, using RT-qPCR and western blotting, the mRNA and protein expression levels of the SG marker G3BP1 were used to quantify SGs, and to detect changes in the expression levels of DDX3X and G3BP1. The protein and mRNA expression levels of both DDX3X and G3BP1 were decreased after 24 h of Dox treatment (Fig. 1C and D). These results indicated that DDX3X expression and SG levels were reduced in Dox-treated H9c2 cells compared with the control.

DDX3X alleviates Dox-induced cardiomyocyte apoptosis and positively regulates SGs. siRNA targeting DDX3X was used to verify the relationship between DDX3X and SGs in DIC, given the similarity in the DDX3X and SG expression changes after Dox treatment. The knockdown efficiency of the DDX3X siRNA in H9c2 cells was verified using RT-qPCR (Fig. 2B). The difference in G3BP1 expression between the DDX3X knockdown and control groups did not considerably differ in the absence of Dox stimulation; however, DDX3X

knockdown exacerbated the decrease in G3BP1 protein levels in the Dox-treated H9c2 cells as well as the reduction in the levels of the anti-apoptotic marker Bcl2 (Fig. 2A). In the rescue experiment, the DDX3X pcDNA3.1-3xFlag-C plasmid was used to transfect H9c2 cells. The RT-qPCR analysis revealed that the mRNA expression levels of DDX3X in the transfected group were increased when compared with those in the control group (Fig. 2C). DDX3X overexpression did not affect the protein expression levels of G3BP1 and Bcl2 in the absence of Dox intervention, whereas DDX3X overexpression reversed the inhibitory effects of Dox on G3BP1 and Bcl2 (Fig. 2D). The DDX3X RNA helicase inhibitor RK-33 did not affect DDX3X protein levels (Fig. 2E). Furthermore, RK-33 did not inhibit G3BP1 protein expression levels in the absence of Dox intervention; however, G3BP1 protein expression levels were reduced in the Dox-treated H9c2 cell group after RK-33 pretreatment, and the protein expression levels of the anti-apoptotic marker Bcl2 were also decreased in the RK-33 + Dox group (Fig. 2E). These results indicated that DDX3X may be a protective factor against DIC and may serve a key regulatory role in the regulation of SGs in Dox-treated H9c2 cells.

SGs ameliorate Dox-induced cardiomyocyte apoptosis. An was used to pretreat H9c2 cells and inhibit SG levels. The G3BP1 protein levels and the expression levels of the anti-apoptotic marker Bcl2 were reduced in the Dox + An group when compared with the Dox group (Fig. 3A). Next, immunofluorescence was used to locate the SGs. Green fluorescence labeled G3BP1 and blue fluorescence labeled the nucleus of H9c2 cells (Fig. 3B). Pretreatment with An exacerbated the reduction in the levels of SGs in Dox-treated H9c2 cells. Our previous study revealed that the apoptosis induced by Dox in H9c2 cells mainly occurred after 12 h (61); therefore, to stimulate SGs formation, H9c2 cells were treated with Ar after 12 h of Dox treatment. A CCK-8 assay was used to measure cell viability because of the cardiotoxicity of Ar. The stimulation of H9c2 cells with 10 μmol/l Ar for 12 h was considered safe (Fig. 3E). Ar treatment reversed the inhibitory effect of Dox on G3BP1 protein levels, and the Bcl2 protein levels did not differ between the Ar and control groups (Fig. 3C). In addition, the stimulation of SGs with Ar upregulated the expression of Bcl2 protein in the Dox
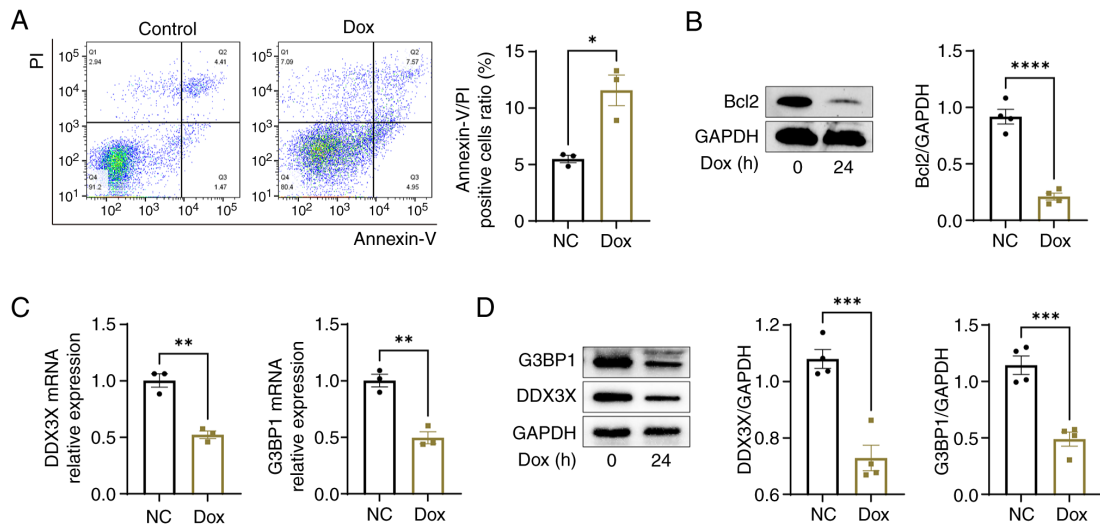
Figure 1. DDX3X and stress granules are downregulated in Dox-induced H9c2 cells. (A) H9c2 cells were treated with Dox (2 μmol/l) for 24 h, and then the apoptosis rate was detected by flow cytometry. (B) Bcl2 protein levels in H9c2 cells treated with Dox (2 μmol/l) for 24 h were analyzed by western blotting. (C) mRNA levels of DDX3X and G3BP1 in Dox (2 μmol/l)-induced H9c2 cells for 24 h were detected by reverse transcription-quantitative PCR. (D) H9c2 cells were treated with Dox (2 μmol/l) for 24 h, and the protein expression levels of DDX3X and G3BP1 were detected by western blotting. Data are presented as the mean ± SEM. Significance was determined by an unpaired Student's t-test. *P≤0.05, **P≤0.01, ***P≤0.001, ****P≤0.0001. Dox, doxorubicin; DDX3X, DEAD-box RNA helicase 3 X-linked; G3BP1, ras GTPase-activating protein-binding protein 1; NC, negative control.
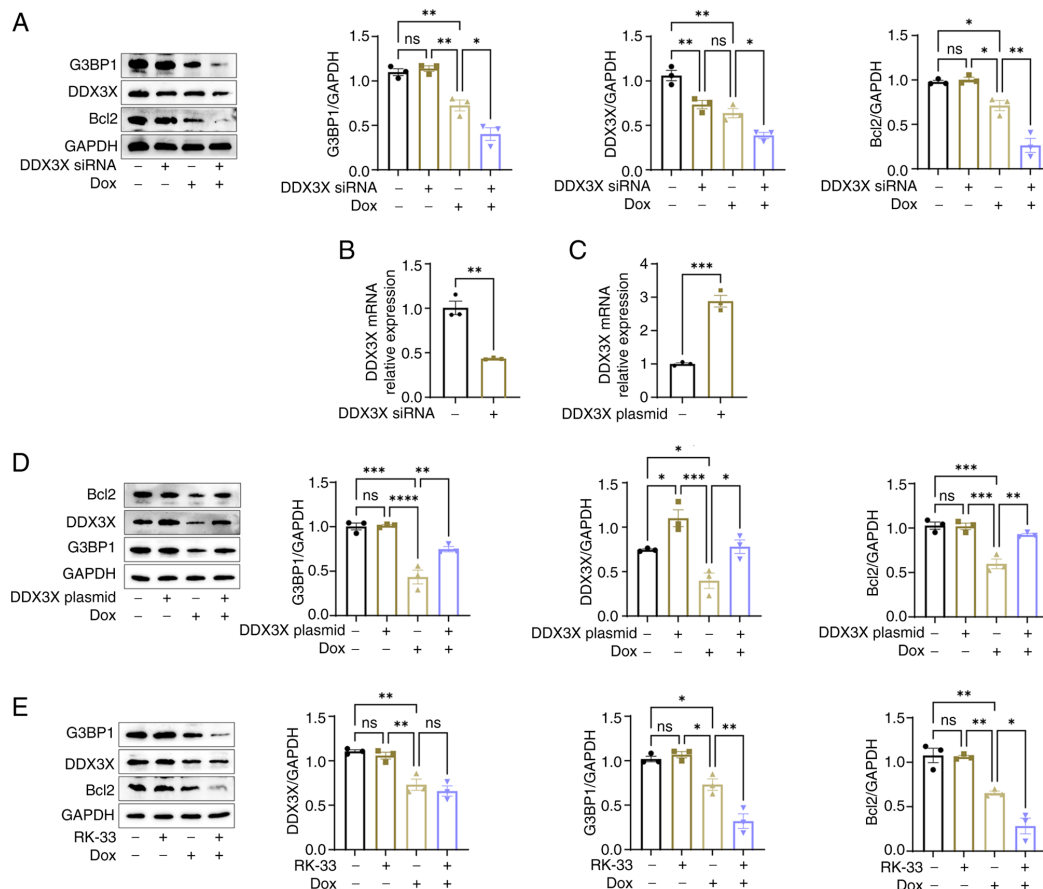

Figure 2. DDX3X alleviates Dox-induced cardiomyocyte apoptosis and positively regulated SGs. (A) H9c2 cells were transfected with DDX3X siRNA, then treated with Dox (2 μmol/l) for 24 h, and the protein changes of DDX3X, G3BP1 and Bcl2 in each group were detected by western blotting. (B) mRNA expression in H9c2 cells transfected with DDX3X siRNA and (C) after DDX3X overexpression was analyzed by reverse transcription-quantitative PCR. (D) H9c2 cells after DDX3X overexpression were treated with Dox (2 μmol/l) for 24 h, and then western blotting was carried out to detect G3BP1, DDX3X and Bcl2 protein expression. (E) H9c2 cells pretreated with RK-33 for 30 min were induced with Dox (2 μmol/l) for 24 h, and the protein expression levels of G3BP1, DDX3X and Bcl2 in each group were detected by western blotting. All experiments were repeated at least three times. Data are presented as the mean ± SEM. Significance was determined by an unpaired Student's t-test (2 groups) or one-way ANOVA with Tukey's multiple comparisons test (≥3 groups), ns, P>0.05, *P≤0.05, **P≤0.01, ***P≤0.001, ****P≤0.0001. Dox, doxorubicin; DDX3X, DEAD-box RNA helicase 3 X-linked; G3BP1, ras GTPase-activating protein-binding protein 1; siRNA, small interfering RNA.
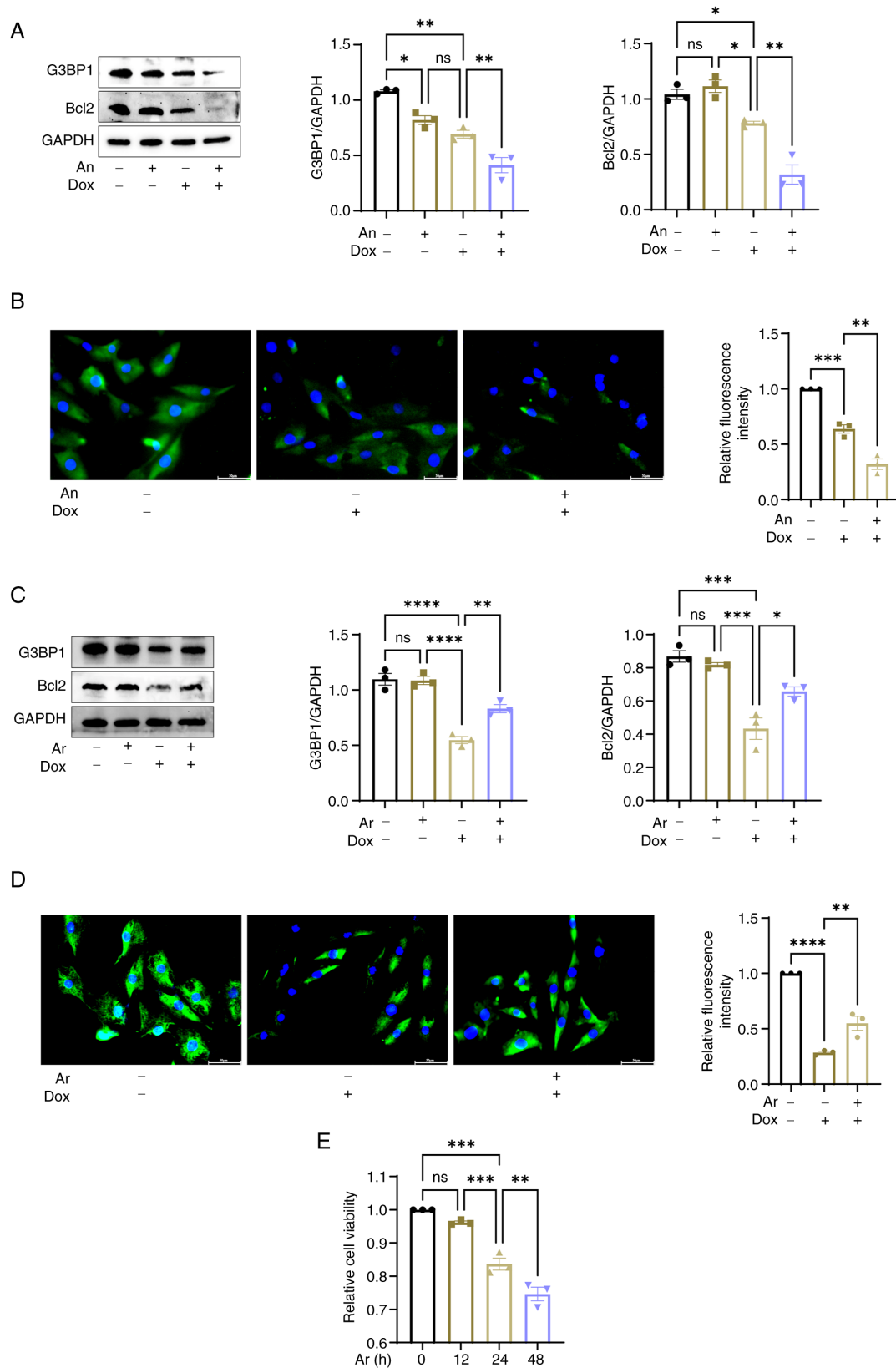
Figure 3. SGs ameliorate Dox-induced cardiomyocyte apoptosis. (A) H9c2 cells pretreated with An were stimulated with Dox (2 μmol/l) for 24 h, and then western blotting was carried out to detect G3BP1 and Bcl2 protein expression. (B) SGs in H9c2 cells induced by Dox (2 μmol/l) for 24 h after An pretreatment were observed by immunofluorescence. SGs were detected using anti-G3BP1 (green) and the nuclei were stained with DAPI (blue). (C) H9c2 cells were first treated with Dox (2 μmol/l) for 12 h, then with Ar in the continued presence of Dox for another 12 h (total Dox exposure: 24 h). Protein levels of G3BP1 and Bcl-2 were analyzed by western blotting. (D) Immunofluorescence was used to observe SGs in H9c2 cells induced by Ar and Dox (2 μmol/l). SGs were detected using anti-G3BP1 (green) and the nuclei were stained with DAPI (blue). Scale bar, 50 μm. (E) Cell viability of H9c2 cells treated with Ar (10 μmol/l) for 0, 12, 24 and 48 h was detected using the Cell Counting Kit-8 assay. All experiments were repeated at least three times. Data are presented as the mean ± SEM. Significance was determined by one-way ANOVA with Tukey's multiple comparisons test. ns, P>0.05, *P≤0.05, **P≤0.01, ***P≤0.001, ****P≤0.0001. Dox, doxorubicin; DDX3X, DEAD-box RNA helicase 3 X-linked; G3BP1, ras GTPase-activating protein-binding protein 1; Ar, arsenite; An, anisomycin; SGs, stress granules.
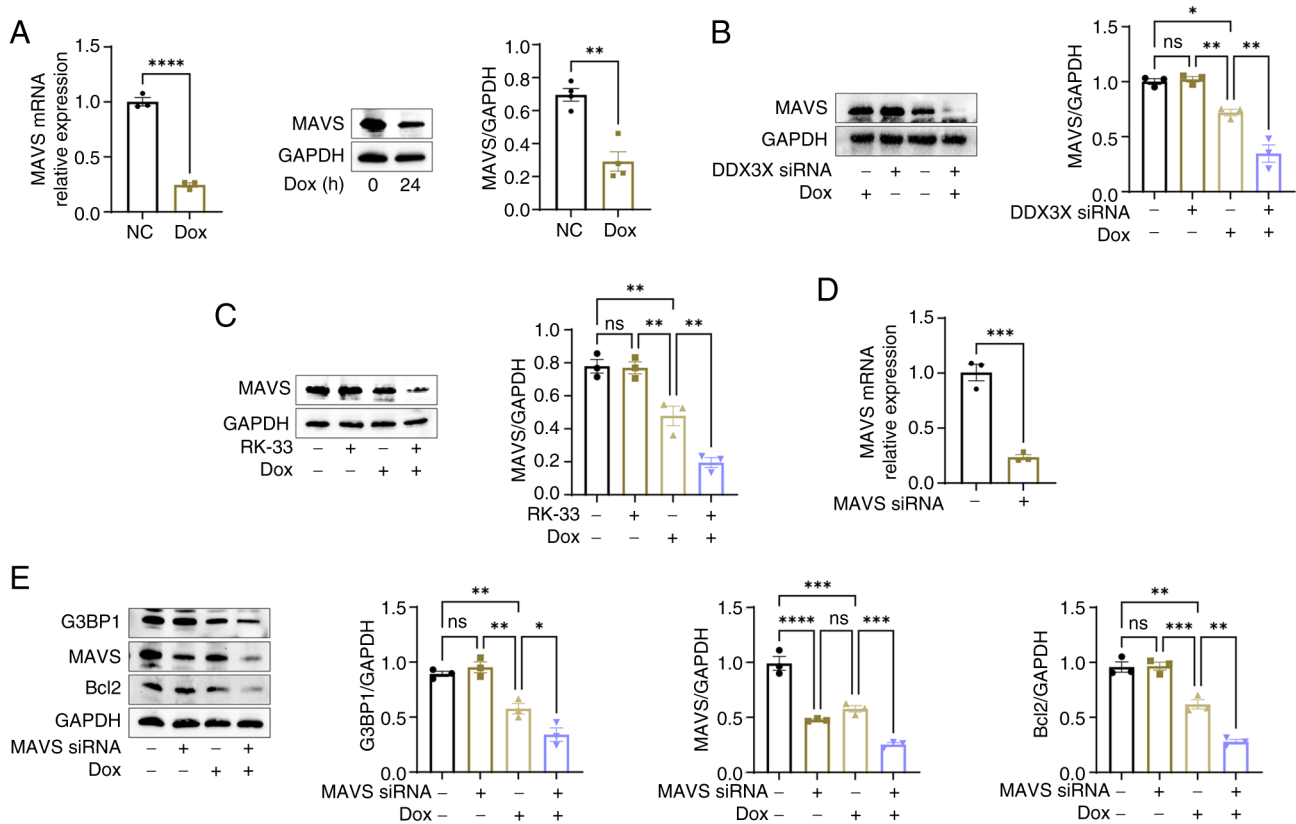
Figure 4. MAVS bridges DDX3X and SGs. (A) mRNA and protein levels of MAVS in H9c2 cells induced by Dox (2 μmol/l) for 24 h were detected by RT-qPCR and western blotting, respectively. (B) H9c2 cells were transfected with DDX3X siRNA, then treated with Dox (2 μmol/l) for 24 h, and the changes in MAVS protein expression in each group were detected by western blotting. (C) H9c2 cells pretreated with RK-33 for 30 min were induced with Dox (2 μmol/l) for 24 h, and then western blotting was carried out to detect MAVS protein expression. (D) Knockdown efficiency of MAVS was determined by RT-qPCR. (E) H9c2 cells transfected with MAVS siRNA were induced with Dox (2 μmol/l) for 24 h, and the protein levels of MAVS, G3BP1 and Bcl2 were determined by western blotting. All experiments were repeated at least three times. Data are presented as the mean ± SEM. Significance was determined by an unpaired Student's t-test (2 groups) or one-way ANOVA with Tukey's multiple comparisons test (≥3 groups). ns, P>0.05, *P≤0.05, **P≤0.01, ***P≤0.001, ****P≤0.0001. Dox, doxorubicin; DDX3X, DEAD-box RNA helicase 3 X-linked; G3BP1, ras GTPase-activating protein-binding protein 1; RT-qPCR, reverse transcription-quantitative PCR; SGs, stress granules; MAVs, mitochondrial antiviral signaling; siRNA, small interfering RNA; NC, negative control.

group. The results of immunofluorescence analysis revealed that the G3BP1 green fluorescence signal in the Dox + Ar group was increased compared with that in the Dox group, indicating that Ar treatment reversed the Dox-induced inhibition of the number of SGs (Fig. 3D). These results indicated that SGs can resist the harmful effects of Dox on H9c2 cells, potentially attenuating Dox-induced myocardial apoptosis.

MAVS bridges DDX3X and SGs. MAVS is a key adapter of the RLR antiviral signaling pathway. Analysis revealed that the mRNA and protein levels of MAVS were decreased in H9c2 cells treated with Dox for 24 h compared with those in the control group (Fig. 4A). DDX3X is the main upstream regulator of MAVS and exerts antiviral effects (36). It was therefore hypothesized that DDDX3X downregulation may inhibit MAVS signaling in DIC because low levels of DDX3X and MAVS were present after Dox treatment. The MAVS protein levels did not differ between the DDX3X siRNA-transfected and control groups, whereas the MAVS protein levels in the Dox + DDX3X siRNA group were substantially decreased compared with those in the Dox group (Fig. 4B). However, whether DDX3X ATPase serves a role in MAVS in DIC remains unknown; therefore, RK-33 (a DDX3X ATPase activity inhibitor) was used to investigate this. RK-33 pretreatment had no effect on MAVS protein

expression in the control group, but aggravated the decrease in MAVS protein levels in the Dox group (Fig. 4C). This result indicated that the ATPase activity of DDX3X is key in the DDX3X regulation of MAVS. The expression of MAVS was inhibited in H9c2 cells by transiently transfecting the cells with MAVS siRNA. Knockdown efficiency of MAVS was verified using RT-qPCR (Fig. 4D). MAVS knockdown intensified the decrease in Bcl2 protein levels in the Dox group (Fig. 4E), suggesting that MAVS may carry out a role in resisting the myocardial damage caused by Dox treatment. Analysis also revealed that the G3BP1 protein levels in the Dox + MAVS siRNA group were reduced when compared with the Dox group, indicating that MAVS may be a key factor promoting SG assembly in DIC (Fig. 4E). The aforementioned results suggested that DDX3X and SGs may require a bridge, MAVS, to connect them in the process of resolving DIC. Fig. 5 shows the potential mechanism through which DDX3X may regulate MAVS and SGs in a model of DIC.

Discussion

Dox damages contractile proteins, such as actin and titin, by stimulating pathways such as the calpain pathway, and it reduces norepinephrine-mediated vasoconstriction through downregulation of α1-adrenergic receptors (62-64). The impact of Dox
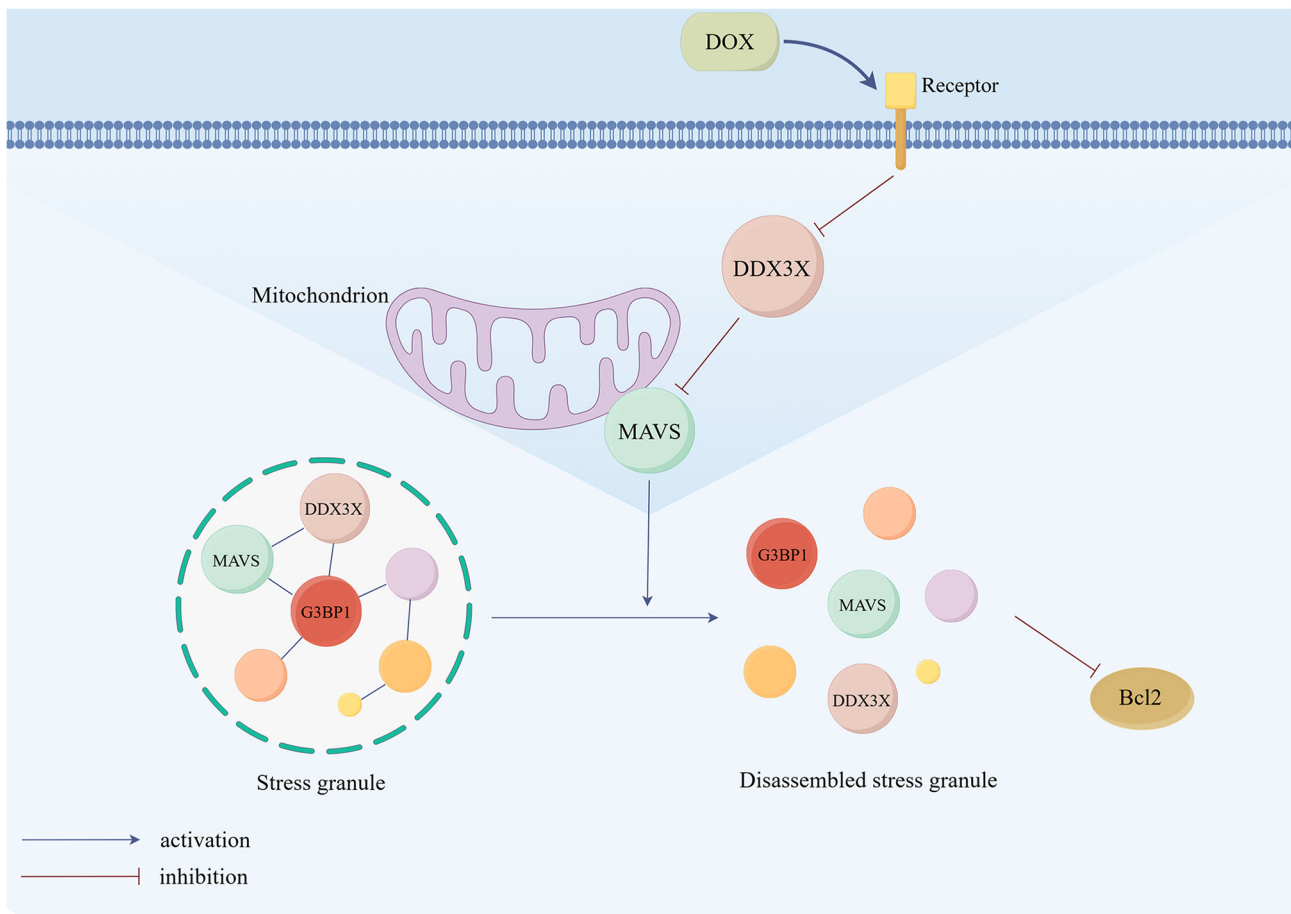
Figure 5. Schematic diagram of the role of DDX3X/MAVS/SGs in Dox-induced cardiotoxicity. When Dox enters cardiomyocytes, the expression of DDX3X is inhibited, which in turn downregulates the expression of the mitochondrial antiviral signal MAVS. The reduction of the DDX3X and MAVS complex inhibits the assembly of SGs, thereby decreasing the production of anti-apoptotic marker Bcl2. Dox, doxorubicin; DDX3X, DEAD-box RNA helicase 3 X-linked; G3BP1, ras GTPase-activating protein-binding protein 1; MAVs, mitochondrial antiviral signaling; SGs, stress granules.

on cardiovascular contractile function eventually leads to acute or chronic heart failure. This effect has limited the application of Dox as a first-line chemotherapeutic agent; therefore, the molecular mechanisms underlying DIC must be identified.

Dox induces cardiotoxicity through various modes of cell death, including apoptosis, pyroptosis and ferroptosis. Topoisomerase (TOP)2β is highly expressed in cardiomyocytes; Dox forms complexes with TOP2β and causes apoptosis by regulating genes such as P53 (65,66). We previously revealed that DDX3X attenuates the Dox-induced apoptosis of H9c2 cardiomyocytes through regulating Wnt/β-catenin signaling (61). The present study revealed that treatment of H9c2 cells with Dox for 24 h downregulated the expression levels of the anti-apoptotic marker Bcl2; increased the apoptosis rate; and decreased the mRNA and protein levels of DDX3X, MAVS and G3BP1. Subsequently, RK-33, Ar, An and siRNAs were used to thoroughly study the relationship between DDX3X/MAVS/SGs and myocardial apoptosis. Finally, the role of DDX3X in alleviating DIC through positively regulating MAVS and SGs was revealed.

SGs have been extensively studied in a variety of neurodegenerative diseases, such as amyotrophic lateral sclerosis. The normal function of SGs is disturbed once pathogenic proteins (such as tau protein) are involved in SG formation, ultimately damaging neurons (67-69). The SGs induced by

chronic persistent stress in neurodegenerative diseases are non-dynamically stable complexes that are difficult to disassemble. The SGs formed under acute stress undergo dynamic and rapid aggregation and dissociation, which promote cell survival (68,70,71). SG levels have been reported to peak at 6 h and reduce to a minimum at 24 h in a rat model of brain tissue ischemia-reperfusion. The apoptosis level and cerebral infarction volume were also revealed to be inversely proportional to SG levels (72).

Ar was used to induce H9c2 cells from the 12 h mark after Dox treatment. The addition of Ar increased the protein expression levels of G3BP1 and anti-apoptotic marker Bcl2 after Dox treatment. Subsequently, H9c2 cells were pretreated with An, which, in contrast to Ar, aggravated DIC by suppressing G3BP1 protein expression levels. An increased number of SGs may thus prevent the damage to cardiomyocytes caused by Dox in the acute stress model. By contrast, a decreased number of SGs could weaken the defensive ability of cardiomyocytes against Dox, which is consistent with SGs being protective against the effects of acute stress.

SGs protect a large number of proteins, as well as mRNAs, and stop translation when cells are damaged through external stressors. SGs antagonize apoptosis by sequestering the receptor for activated protein C kinase 1 and other factors (73,74). This may be a mechanism through which SGs mitigate the effects

of DIC. The heart lacks antioxidant enzymes such as superoxide dismutase and catalase (75,76), whereas Dox produces ROS and superoxide anions by inducing oxidative stress in cardiomyocytes, which further weakens the defensive abilities of cardiomyocytes (77,78). The core protein G3BP1 of SGs can weaken the inhibition of the antioxidant enzyme USP10 under the stressed state induced by Ar and other stimulants, thus reducing the production of ROS and levels of apoptosis (79). SG levels were reported to peak after 6 h of pacing in a cardiomyocyte model of atrial fibrillation, and G3BP1 overexpression were revealed to decrease ROS levels induced by rapid pacing (54). Therefore, the antioxidant effect of SGs and ROS downregulation may be additional mechanisms by which increased SG levels resolve DIC.

The gene encoding DDX3X is located on p11.3-11.23 of the X chromosome and is widely expressed in the majority of tissues, including the myocardium and blood vessels (80). DDX3X induces neural crest development by promoting RAC1/AKT (81). DDX3X mutations occur in 1-3% of women with unexplained intellectual disability (82). Molina-Navarro et al (83) tested the genetic sequences of 31 patients undergoing heart transplant and revealed that DDX3X is related to ischemic cardiomyopathy.

RK-33 is a small-molecule DDX3X inhibitor that functions by inhibiting the ATP-binding domain of DDX3X. RK-33 is expected to become a broad-spectrum antiviral agent because it can effectively treat SARS-CoV-2 (84). The anti-apoptotic protein Bcl2 was significantly downregulated compared with that in the Dox group when H9c2 cells were treated with RK-33 for 30 min before Dox, which suggests that the ATP domain of DDX3X may be key in DIC regulation by DDX3X. In the present study, H9c2 cells were transfected with DDX3X siRNA before Dox treatment, which revealed that DDX3X knockdown intensified Bcl2 downregulation in the Dox group. Conversely, DDX3X overexpression reversed the inhibitory effect of Dox on Bcl2. These results indicated that DDX3X may be a protective gene against DIC that serves an important role in the pathological mechanism of DIC, providing ideas for the treatment of cardiac dysfunction caused by Dox.

Hepatitis C induces the production of SGs through DDX3X to promote their expression and replication (85). In addition, G3BP1 and DDX3X are necessary for effective SARS-CoV-2 replication (86,87). DDX3X deficiency in non-alcoholic steatohepatitis obstructs SG assembly and activates the pyroptosis marker, NLRC4, exacerbating the progression of hepatitis (88). The present study demonstrated that DDX3X knockdown and RK-33-mediated inhibition of DDX3X ATPase activity reduced G3BP1 protein expression levels in the Dox-treated group, whereas DDX3X overexpression increased G3BP1 protein expression levels in the Dox treatment group. These findings indicated that DDX3X may also be a key factor in the SG assembly process in DIC, with ATPase activity being key to this process. It could be hypothesized that Dox induces myocardial damage by inhibiting DDX3X to decrease SG production.

DDX3X, an RNA helicase, may manage the RNA encapsulated within SGs through its ATPase activity, thereby assisting SGs in protecting RNA. HDAC6 deacetylates the intrinsically disordered region of DDX3X to enhance LLPS propensity, which is necessary for SG maturation (45). DDX3X and G3BP1 interact with their RG/RGG domains and subsequently bind eIF4A, inducing SG formation (89). Thus, DDX3X may promote SG formation in DIC by regulating LLPS and physically combining with G3BP1 to stabilize the SGs. This may be the mechanism through which DDX3X regulates SGs in the DIC model. The regulation of the compositional factors of SGs will be a key approach in future research on SGs.

MAVS is a key line of defense against viral infections. RIG-I/MAVS/TRAF is an antiviral signaling pathway, which participates in the natural immune response triggered by numerous viruses (90). MAVS protects cardiac function and promotes myocardial remodeling (39). In the present study, MAVS knockdown downregulated Bcl2 protein expression in the Dox-treated group, indicating that MAVS resists Dox-induced myocardial apoptosis and verifying that MAVS is an important protective factor against DIC.

Dox forms an irreversible complex with cardiolipin in the mitochondrial membrane, increasing oxide production (91,92). Knocking out MAVS in cardiomyocytes can destroy the mitochondrial structure and increase ROS production in the mitochondria (93). In addition, Dox causes an imbalance in glucose and fatty acid metabolism in the mitochondria (94), whereas MAVS knockout increases fat accumulation in cells (95). Therefore, MAVS may alleviate DIC by protecting mitochondrial function and increasing cardiomyocyte metabolism.

DDX3X promotes interferon production via regulating MAVS after viral stimulation, and MAVS also activates the host antiviral response via promoting SG formation (37). Therefore, it was hypothesized that MAVS carries out a role in protecting DDX3X and SGs against DIC. Analysis revealed that DDX3X knockdown and the RK-33-induced inhibition of DDX3X ATPase activity both decreased the levels of MAVS in the Dox-treated group, whereas MAVS knockdown exacerbated the reduction in G3BP1 protein expression levels induced by Dox treatment, suggesting that MAVS may bridge the SG assembly promoted by DDX3X in the DIC model.

DDX3X has been shown to directly bind to the caspase activation and recruitment domain of MAVS to promote MAVS activation (36), and activated MAVS co-localizes with the core SG proteins (38). DDX3X may therefore physically interact with MAVS in DIC, and the DDX3X-MAVS complex could facilitate SG formation through stabilizing core proteins such as G3BP1.

In summary, the present study validated that the DDX3X/MAVS/SGs signaling pathway may be involved in the occurrence of DIC. DDX3X could mitigate the damage caused by Dox treatment on cardiomyocytes by regulating MAVS and SG depolymerization. Notably, it was suggested that the ATPase activity of DDX3X may serve a key role in this process. The present study not only expands the understanding of the mechanisms of DIC but also provides novel information for future DIC treatment.

The present study also has limitations. The protective effect of DDX3X/MAVS/SGs on DIC was only verified at the cellular level and this conclusion was not studied using further in vivo experiments. Although analysis revealed that DDX3X downregulated MAVS and SGs in the DIC model, the specific regulatory mechanism requires further exploration. Therefore, a comprehensive investigation of the specific mechanisms through which

DDX3X regulates MAVS and SGs in DIC through cellular and animal experiments will be the key focus of future research. Additionally, determining the optimal timing for targeting SGs and elucidating the precise mechanisms of SG formation are also key areas for future studies because the SGs formed under acute stress are dynamic and unstable.

Availability of data and materials

The data generated in the present study may be requested from the corresponding author.

Authors' contributions

KZ, SW, DF, DW, GY and FL were involved in the study design. KZ and SW performed the experiments. KZ analyzed the data and drafted the initial manuscript. KZ and GY confirm the authenticity of all the raw data. All authors have read and approved the final manuscript.

Ethics approval and consent to participate

Not applicable.

Patient consent for publication

Not applicable.

Competing interests

The authors declare that they have no competing interests.

References

1. Momparler RL, Karon M, Siegel SE and Avila F: Effect of adriamycin on DNA, RNA, and protein synthesis in cell-free systems and intact cells. Cancer Res 36: 2891-2895.
2. Fornari FA, Randolph JK, Yalowich JC, Ritke MK and Gewirtz DA: Interference by doxorubicin with DNA unwinding in MCF-7 breast tumor cells. Mol Pharmacol 45: 649-656, 1994.
3. Pommier Y, Capranico G, Orr A and Kohn KW: Local base sequence preferences for DNA cleavage by mammalian topoisomerase II in the presence of amsacrine or teniposide. Nucleic Acids Res 19: 5973-5980, 1991.
4. Tewey KM, Rowe TC, Yang L, Halligan BD and Liu LF: Adriamycin-induced DNA damage mediated by mammalian DNA topoisomerase II. Science 226: 466-468, 1984.
5. Zamorano JL, Lancellotti P, Rodriguez Muñoz D, Aboyans V, Asteggiano R, Galderisi M, Habib G, Lenihan DJ, Lip GYH, Lyon AR, *et al*: 2016 ESC Position Paper on cancer treatments and cardiovascular toxicity developed under the auspices of the ESC Committee for Practice Guidelines: The Task Force for cancer treatments and cardiovascular toxicity of the European Society of Cardiology (ESC). Eur Heart J 37: 2768-2801, 2016.
6. Cui L, Huang J, Zhan Y, Qiu N, Jin H, Li J, Huang H and Li H: Association between the genetic polymorphisms of the pharmacokinetics of anthracycline drug and myelosuppression in a patient with breast cancer with Anthracycline-based chemotherapy. Life Sci 276: 119392, 2021.
7. Ramalingayya GV, Cheruku SP, Nayak PG, Kishore A, Shenoy R, Rao CM and Krishnadas N: Rutin protects against neuronal damage in vitro and ameliorates doxorubicin-induced memory deficits in vivo in Wistar rats. Drug Des Devel Ther 11: 1011-1026, 2017.
8. Dean JC, Salmon SE and Griffith KS: Prevention of doxorubicin-induced hair loss with scalp hypothermia. N Engl J Med 301: 1427-1429, 1979.
9. Swain SM, Whaley FS and Ewer MS: Congestive heart failure in patients treated with doxorubicin: A retrospective analysis of three trials. Cancer 97: 2869-2879, 2003.
10. Fornaro A, Olivotto I, Rigacci L, Ciaccheri M, Tomberli B, Ferrantini C, Coppini R, Girolami F, Mazzarotto F and Chiostri M: Comparison of long-term outcome in anthracycline-related versus idiopathic dilated cardiomyopathy: A single centre experience. Eur J Heart Fail 20: 898-906, 2018.
11. Cardinale D, Colombo A, Bacchiani G, Tedeschi I, Meroni CA, Veglia F, Civelli M, Lamantia G, Colombo N, Curigliano G, *et al*: Early detection of anthracycline cardiotoxicity and improvement with heart failure therapy. Circulation 131: 1981-1988, 2015.
12. Berthiaume JM and Wallace KB: Adriamycin-induced oxidative mitochondrial cardiotoxicity. Cell Biology Toxicol 23: 15-25, 2006.
13. Goormaghtigh E, Huart P, Praet M, Brasseur R and Ruysschaert JM: Structure of the adriamycin-cardiolipin complex. Role in mitochondrial toxicity. Biophys Chem 35: 247-257, 1990.
14. Hoye AT, Davoren JE, Wipf P, Fink MP and Kagan VE: Targeting mitochondria. Acc Chem Res 41: 87-97, 2008.
15. Chen Y, Jungsuwadee P, Vore M, Butterfield DA and St Clair DK: Collateral damage in cancer chemotherapy: Oxidative stress in nontargeted tissues. Mol Interv 7: 147-156, 2007.
16. Deng S, Kruger A, Kleschyov AL, Kalinowski L, Daiber A and Wojnowski L: Gp91phox-containing NAD(P)H oxidase increases superoxide formation by doxorubicin and NADPH. Free Radic Biol Med 42: 466-473, 2007.
17. Doroshow JH, Esworthy RS and Chu FF: Control of doxorubicin-induced, reactive oxygen-related apoptosis by glutathione peroxidase 1 in cardiac fibroblasts. Biochem Biophys Rep 21: 100709, 2020.
18. Kong CY, Guo Z, Song P, Zhang X, Yuan YP, Teng T, Yan L and Tang QZ: Underlying the mechanisms of doxorubicin-induced acute cardiotoxicity: Oxidative stress and cell death. Int J Biol Sci 18: 760-770, 2022.
19. Xiong Y, Liu X, Lee CP, Chua BHL and Ho YS: Attenuation of doxorubicin-induced contractile and mitochondrial dysfunction in mouse heart by cellular glutathione peroxidase. Free Radic Biol Med 41: 46-55, 2006.
20. Sharma D and Jankowsky E: The Ded1/DDX3 subfamily of DEAD-box RNA helicases. Crit Rev Biochem Mol Biol 49: 343-360, 2014.
21. Högbom M, Collins R, van den Berg S, Jenvert RM, Karlberg T, Kotenyova T, Flores A, Karlsson Hedestam GB and Schiavone LH: Crystal structure of conserved domains 1 and 2 of the human DEAD-box helicase DDX3X in complex with the mononucleotide AMP. J Mol Biol 372: 150-159, 2007.
22. Tantravedi S, Vesuna F, Winnard PT Jr, Van Voss MRH, Van Diest PJ and Raman V: Role of DDX3 in the pathogenesis of inflammatory bowel disease. Oncotarget 8: 115280-115289, 2017.
23. Schröder M: Viruses and the human DEAD-box helicase DDX3: Inhibition or exploitation? Biochem Soc Trans 39: 679-683, 2011.
24. Linder P and Jankowsky E: From unwinding to clamping-the DEAD box RNA helicase family. Nat Rev Mol Cell Biol 12: 505-516, 2011.
25. Lee CS, Dias AP, Jedrychowski M, Patel AH, Hsu JL and Reed R: Human DDX3 functions in translation and interacts with the translation initiation factor eIF3. Nucleic Acids Res 36: 4708-4718, 2008.
26. Kellaris G, Khan K, Baig SM, Tsai IC, Zamora FM, Ruggieri P, Natowicz MR and Katsanis N: A hypomorphic inherited pathogenic variant in DDX3X causes male intellectual disability with additional neurodevelopmental and neurodegenerative features. Hum Genomics 12: 11, 2018.
27. Jankowsky A, Guenther UP and Jankowsky E: The RNA helicase database. Nucleic Acids Res 39: D338-D341, 2011.

28. Lai MC, Lee YH and Tarn WY: The DEAD-box RNA helicase DDX3 associates with export messenger ribonucleoproteins as well as tip-associated protein and participates in translational control. Mol Biol Cell 19: 3847-3858, 2008.
29. Brennan R, Haap-Hoff A, Gu L, Gautier V, Long A and Schröder M: Investigating nucleo-cytoplasmic shuttling of the human DEAD-box helicase DDX3. Eur J Cell Biol 97: 501-511, 2018.
30. Chen HH, Yu HI, Cho WC and Tarn WY: DDX3 modulates cell adhesion and motility and cancer cell metastasis via Rac1-mediated signaling pathway. Oncogene 34: 2790-2800, 2015.
31. Valentin-Vega YA, Wang YD, Parker M, Patmore DM, Kanagaraj A, Moore J, Rusch M, Finkelstein D, Ellison DW, Gilbertson RJ, et al: Cancer-associated DDX3X mutations drive stress granule assembly and impair global translation. Sci Rep 6: 25996, 2016.
32. Soulat D, Bürckstümmer T, Westermayer S, Goncalves A, Bauch A, Stefanovic A, Hantschel O, Bennett KL, Decker T and Superti-Furga G: The DEAD-box helicase DDX3X is a critical component of the TANK-binding kinase 1-dependent innate immune response. EMBO J 27: 2135-2146, 2008.
33. Kienes I, Bauer S, Gottschild C, Mirza N, Pfannstiel J, Schröder M and Kufer TA: DDX3X links NLRP11 to the regulation of type I interferon responses and NLRP3 inflammasome activation. Front Immunol 12: 653883, 2021.
34. Gu L, Fullam A, Brennan R and Schröder M: Human DEAD box helicase 3 couples IκB kinase ε to interferon regulatory factor 3 activation. Mol Cell Biol 33: 2004-2015, 2013.
35. Samir P, Kesavardhana S, Patmore DM, Gingras S, Malireddi RKS, Karki R, Guy CS, Briard B, Place DE, Bhattacharya A, et al: DDX3X acts as a live-or-die checkpoint in stressed cells by regulating NLRP3 inflammasome. Nature 573: 590-594, 2019.
36. Oshiumi H, Sakai K, Matsumoto M and Seya T: DEAD/H BOX 3 (DDX3) helicase binds the RIG-I adaptor IPS-1 to up-regulate IFN-beta-inducing potential. Eur J Immunol 40: 940-948, 2010.
37. Zhang P, Li Y, Xia J, He J, Pu J, Xie J, Wu S, Feng L, Huang X and Zhang P: IPS-1 plays an essential role in dsRNA-induced stress granule formation by interacting with PKR and promoting its activation. J Cell Sci 127: 2471-2482, 2014.
38. Aoyama-Ishiwatari S, Okazaki T, Iemura SI, Natsume T, Okada Y and Gotoh Y: NUDT21 links mitochondrial IPS-1 to RLR-containing stress granules and activates host antiviral defense. J Immunol 206: 154-163, 2021.
39. Lin HB, Naito K, Oh Y, Farber G, Kanaan G, Valaperti A, Dawood F, Zhang L, Li GH, Smyth D, et al: Innate Immune Nod1/RIP2 signaling is essential for cardiac hypertrophy but requires mitochondrial antiviral signaling protein for signal transductions and energy balance. Circulation 142: 2240-2258, 2020.
40. Li WY, Yang F, Li X, Wang LW and Wang Y: Stress granules inhibit endoplasmic reticulum stress-mediated apoptosis during hypoxia-induced injury in acute liver failure. World J Gastroenterol 29: 1315-1329, 2023.
41. Anderson P and Kedersha N: RNA granules: Post-transcriptional and epigenetic modulators of gene expression. Nat Rev Mol Cell Biol 10: 430-436, 2009.
42. Kedersha N, Stoecklin G, Ayodele M, Yacono P, Lykke-Andersen J, Fritzler MJ, Scheuner D, Kaufman RJ, Golan DE and Anderson P: Stress granules and processing bodies are dynamically linked sites of mRNP remodeling. J Cell Biol 169: 871-884, 2005.
43. Protter DSW and Parker R: Principles and properties of stress granules. Trends Cell Biol 26: 668-679, 2016.
44. Molliex A, Temirov J, Lee J, Coughlin M, Kanagaraj AP, Kim HJ, Mittag T and Taylor JP: Phase separation by low complexity domains promotes stress granule assembly and drives pathological fibrillization. Cell 163: 123-133, 2015.
45. Saito M, Hess D, Eglinger J, Fritsch AW, Kreysing M, Weinert BT, Choudhary C and Matthias P: Acetylation of intrinsically disordered regions regulates phase separation. Nat Chem Biol 15: 51-61, 2019.
46. Wheeler JR, Matheny T, Jain S, Abrisch R and Parker R: Distinct stages in stress granule assembly and disassembly. Elife 5: e18413, 2016.
47. Jain S, Wheeler JR, Walters RW, Agrawal A, Barsic A and Parker R: ATPase-modulated stress granules contain a diverse proteome and substructure. Cell 164: 487-498, 2016.
48. Zhao J, Fu X, Chen H, Min L, Sun J, Yin J, Guo J, Li H, Tang Z, Ruan Y, et al: G3BP1 interacts with YWHAZ to regulate chemoresistance and predict adjuvant chemotherapy benefit in gastric cancer. Br J Cancer 124: 425-436, 2021.
49. Wang X, Chen T, Li C, Li W, Zhou X, Li Y, Luo D, Zhang N, Chen B, Wang L, et al: CircRNA-CREIT inhibits stress granule assembly and overcomes doxorubicin resistance in TNBC by destabilizing PKR. J Hematol Oncol 15: 122, 2022.
50. Oh SW, Onomoto K, Wakimoto M, Onoguchi K, Ishidate F, Fujiwara T, Yoneyama M, Kato H and Fujita T: Leader-containing uncapped viral transcript activates RIG-I in antiviral stress granules. PLoS Pathog 12: e1005444, 2016.
51. Li YR, King OD, Shorter J and Gitler AD: Stress granules as crucibles of ALS pathogenesis. J Cell Biol 201: 361-372, 2013.
52. Moraes KC, Monteiro CJ and Pacheco-Soares C: A novel function for CUGBP2 in controlling the pro-inflammatory stimulus in H9c2 cells: Subcellular trafficking of messenger molecules. Cell Biol Int 37: 1129-1138, 2013.
53. Alikunju S, Niranjan N, Mohsin M, Sayed N and Sayed D: G3bp1-microRNA-1 axis regulates cardiomyocyte hypertrophy. Cell Signal 91: 110245, 2022.
54. Dong G, Liang F, Sun B, Wang C, Liu Y, Guan X, Yang B, Xiu C, Yang N, Liu F, et al: Presence and function of stress granules in atrial fibrillation. PLoS One 14: e0213769, 2019.
55. Wang Y, Liu R, Wu K, Yang G, Wang Y, Wang H and Rui T: Stress granule activation attenuates lipopolysaccharide-induced cardiomyocyte dysfunction. BMC Cardiovasc Disord 23: 277, 2023.
56. Guo Y, Hinchman MM, Lewandrowski M, Cross ST, Sutherland DM, Welsh OL, Dermody TS and Parker JSL: The multi-functional reovirus σ3 protein is a virulence factor that suppresses stress granule formation and is associated with myocardial injury. PLoS Pathog 17: e1009494, 2021.
57. Livak KJ and Schmittgen TD: Analysis of relative gene expression data using Real-time quantitative PCR and the 2(-Delta Delta C(T)) method. Methods 25: 402-408, 2001.
58. Jiang Y, Liu Y, Xiao W, Zhang D, Liu X, Xiao H, You S and Yuan L: Xinmailong Attenuates Doxorubicin-induced lysosomal dysfunction and oxidative stress in H9c2 cells via HO-1. Oxid Med Cell Longev 2021: 5896931, 2021.
59. Zhang H, Pan J, Huang S, Chen X, Chang ACY, Wang C, Zhang J and Zhang H: Hydrogen sulfide protects cardiomyocytes from doxorubicin-induced ferroptosis through the SLC7A11/GSH/GPx4 pathway by Keap1 S-sulfhydration and Nrf2 activation. Redox Biology 70: 103066, 2024.
60. Hu C, Zhang X, Song P, Yuan YP, Kong C-Y, Wu HM, Xu SC, Ma ZG and Tang QZ: Meteorin-like protein attenuates doxorubicin-induced cardiotoxicity via activating cAMP/PKA/SIRT1 pathway. Redox Biology 37: 101747, 2020.
61. Feng D, Li J, Guo L, Liu J, Wang S, Ma X, Song Y, Liu J and Hao E: DDX3X alleviates doxorubicin-induced cardiotoxicity by regulating Wnt/β-catenin signaling pathway in an in vitro model. J Biochem Mol Toxicol 36: e23077, 2022.
62. Rawat PS, Jaiswal A, Khurana A, Bhatti JS and Navik U: Doxorubicin-induced cardiotoxicity: An update on the molecular mechanism and novel therapeutic strategies for effective management. Biomed Pharmacother 139: 111708, 2021.
63. Lim CC, Zuppinger C, Guo X, Kuster GM, Helmes M, Eppenberger HM, Suter TM, Liao R and Sawyer DB: Anthracyclines induce calpain-dependent titin proteolysis and necrosis in cardiomyocytes. J Biol Chem 279: 8290-8299, 2004.
64. Ahmadiasl N, Rostami A, Mohammadi NM and Rajabi F: Effects of noradrenaline and KCl on peripheral vessels in doxorubicin induced model of heart failure. Pathophysiology 8: 259-262, 2002.
65. Lin RW, Ho CJ, Chen HW, Pao YH, Chen LE, Yang MC, Huang SB, Wang S, Chen CH and Wang C: P53 enhances apoptosis induced by doxorubicin only under conditions of severe DNA damage. Cell Cycle 17: 2175-2186, 2018.
66. Cui N, Wu F, Lu WJ, Bai R, Ke B, Liu T, Li L, Lan F and Cui M: Doxorubicin-induced cardiotoxicity is maturation dependent due to the shift from topoisomerase IIα to IIβ in human stem cell derived cardiomyocytes. J Cell Mol Med 23: 4627-4639, 2019.
67. Zhang X, Wang F, Hu Y, Chen R, Meng D, Guo L, Lv H, Guan J and Jia Y: In vivo stress granule misprocessing evidenced in a FUS knock-in ALS mouse model. Brain 143: 1350-1367, 2020.
68. Wolozin B and Ivanov P: Stress granules and neurodegeneration. Nat Rev Neurosci 20: 649-666, 2019.
69. Cui Q, Bi H, Lv Z, Wu Q, Hua J, Gu B, Huo C, Tang M, Chen Y, Chen C, et al: Diverse CMT2 neuropathies are linked to aberrant G3BP interactions in stress granules. Cell 186: 803-820.e25, 2023.
70. Asadi MR, Sadat Moslehian M, Sabaie H, Jalaiei A, Ghafouri-Fard S, Taheri M and Rezazadeh M: Stress granules and neurodegenerative disorders: A scoping review. Front Aging Neurosci 13: 650740, 2021.

71. Arimoto K, Fukuda H, Imajoh-Ohmi S, Saito H and Takekawa M: Formation of stress granules inhibits apoptosis by suppressing stress-responsive MAPK pathways. Nat Cell Biol 10: 1324-1332, 2008.

72. Si W, Ye S, Ren Z, Liu X, Wu Z, Li Y, Zhou J, Zhang S, Li Y, Deng R and Chen D: miR-335 promotes stress granule formation to inhibit apoptosis by targeting ROCK2 in acute ischemic stroke. Int J Mol Med 43: 1452-1466, 2019.

73. Kedersha N, Ivanov P and Anderson P: Stress granules and cell signaling: More than just a passing phase? Trends Biochem Sci 38: 494-506, 2013.

74. Thedieck K, Holzwarth B, Prentzell MT, Boehlke C, Kläsener K, Ruf S, Sonntag AG, Maerz L, Grellscheid SN, Kremmer E, *et al*: Inhibition of mTORC1 by astrin and stress granules prevents apoptosis in cancer cells. Cell 154: 859-874, 2013.

75. Doroshow JH, Locker GY and Myers CE: Enzymatic defenses of the mouse heart against reactive oxygen metabolites: Alterations produced by doxorubicin. J Clin Invest 65: 128-1235, 1980.

76. do Nascimento TC, Cazarin CBB, Maróstica MR Jr, Mercadante AZ, Jacob-Lopes E and Zepka LQ: Microalgae carotenoids intake: Influence on cholesterol levels, lipid peroxidation and antioxidant enzymes. Food Res Int 128: 108770, 2020.

77. Mihm MJ, Yu F, Weinstein DM, Reiser PJ and Bauer JA: Intracellular distribution of peroxynitrite during doxorubicin cardiomyopathy: Evidence for selective impairment of myofibrillar creatine kinase. Br J Pharmacol 135: 581-588, 2002.

78. Deavall DG, Martin EA, Horner JM and Roberts R: Drug-induced oxidative stress and toxicity. J Toxicol 2012: 645460, 2012.

79. Takahashi M, Higuchi M, Matsuki H, Yoshita M, Ohsawa T, Oie M and Fujii M: Stress granules inhibit apoptosis by reducing reactive oxygen species production. Mol Cell Biol 33: 815-829, 2013.

80. Kim YS, Lee SG, Park SH and Song K: Gene structure of the human DDX3 and chromosome mapping of its related sequences. Mol Cells 12: 209-214, 2001.

81. Perfetto M, Xu X, Lu C, Shi Y, Yousaf N, Li J, Yien YY and Wei S: The RNA helicase DDX3 induces neural crest by promoting AKT activity. Development 148: dev184341, 2021.

82. Snijders Blok L, Madsen E, Juusola J, Gilissen C, Baralle D, Reijnders MR, Venselaar H, Helsmoortel C, Cho MT, Hoischen A, *et al*: Mutations in DDX3X Are a common cause of unexplained intellectual disability with Gender-specific effects on wnt signaling. Am J Hum Genet 97: 343-352, 2015.

83. Molina-Navarro MM, Triviño JC, Martínez-Dolz L, Lago F, González-Juanatey JR, Portolés M and Rivera M: Functional networks of nucleocytoplasmic transport-related genes differentiate ischemic and dilated cardiomyopathies. A new therapeutic opportunity. PLoS One 9: e104709, 2014.

84. Vesuna F, Akhrymuk I, Smith A, Winnard PT Jr, Lin SC, Panny L, Scharpf R, Kehn-Hall K and Raman V: RK-33, a small molecule inhibitor of host RNA helicase DDX3, suppresses multiple variants of SARS-CoV-2. Front Microbiol 13: 959577, 2022.

85. Pène V, Li Q, Sodroski C, Hsu CS and Liang TJ: Dynamic interaction of stress granules, DDX3X, and IKK-α mediates multiple functions in Hepatitis C virus infection. J Virol 89: 5462-5477, 2015.

86. He S, Gou H, Zhou Y, Wu C, Ren X, Wu X, Guan G, Jin B, Huang J, Jin Z and Zhao T: The SARS-CoV-2 nucleocapsid protein suppresses innate immunity by remodeling stress granules to atypical foci. FASEB J 37: e23269, 2023.

87. Ciccosanti F, Di Rienzo M, Romagnoli A, Colavita F, Refolo G, Castilletti C, Agrati C, Brai A, Manetti F, Botta L, *et al*: Proteomic analysis identifies the RNA helicase DDX3X as a host target against SARS-CoV-2 infection. Antiviral Res 190: 105064, 2021.

88. Yang S, Zhou L, Zhao T, Zhu H, Luo T, Jiang K, Shi X, Chen C, Zhang H, Zhao S, *et al*: Protective and adverse roles of DDX3X in different cell types in nonalcoholic steatohepatitis progression. Research (Wash D C) 6: 0275, 2023.

89. Chen H, Li B, Zhao X, Yang C, Zhou S and Ma W: Cell-free analysis reveals the role of RG/RGG motifs in DDX3X phase separation and their potential link to cancer pathogenesis. Int J Biol Macromol 279: 135251, 2024.

90. Gu L, Fullam A, McCormack N, Höhn Y and Schröder M: DDX3 directly regulates TRAF3 ubiquitination and acts as a scaffold to co-ordinate assembly of signalling complexes downstream from MAVS. Biochem J 474: 571-587, 2017.

91. Ventura-Clapier R, Garnier A and Veksler V: Energy metabolism in heart failure. J Physiol 555: 1-13, 2004.

92. Oliveira PJ and Wallace KB: Depletion of adenine nucleotide translocator protein in heart mitochondria from doxorubicin-treated rats-relevance for mitochondrial dysfunction. Toxicology 220: 160-168, 2006.

93. Wang Q, Sun Z, Cao S, Lin X, Wu M, Li Y, Yin J, Zhou W, Huang S, Zhang A, *et al*: Reduced immunity regulator MAVS contributes to Non-hypertrophic cardiac dysfunction by disturbing energy metabolism and mitochondrial homeostasis. Front Immunol 13: 919038, 2022.

94. Carvalho RA, Sousa RP, Cadete VJ, Lopaschuk GD, Palmeira CM, Bjork JA and Wallace KB: Metabolic remodeling associated with subchronic doxorubicin cardiomyopathy. Toxicology 270: 92-98, 2010.

95. Fu J, Hu F, Ma T, Zhao WJ, Tian H, Zhang Y, Hu M, Zhou J, Zhang Y, Jian C, *et al*: A conventional immune regulator mitochondrial antiviral signaling protein blocks hepatic steatosis by maintaining mitochondrial homeostasis. Hepatology 75: 403-418, 2022.